Road Materials and Pavement Design

ISSN: (Print) (Online) Journal homepage: https://www.tandfonline.com/loi/trmp20

Evaluation of cracking resistance of healed warm mix asphalt based on air-void and binder content

Tam Minh Phan , Tri Ho Minh Le & Dae-Wook Park

To cite this article: Tam Minh Phan , Tri Ho Minh Le & Dae-Wook Park (2020): Evaluation of cracking resistance of healed warm mix asphalt based on air-void and binder content, Road Materials and Pavement Design, DOI: 10.1080/14680629.2020.1829010

To link to this article: https://doi.org/10.1080/14680629.2020.1829010

Published online: 12 Oct 2020.

ROAD MATERIALS AND PAVEMENT DESIGN
https://doi.org/10.1080/14680629.2020.1829010

Taylor & Francis
Taylor & Francis Group

Evaluation of cracking resistance of healed warm mix asphalt based on air-void and binder content

Tam Minh Phan, Tri Ho Minh Le and Dae-Wook Park

Department of Civil Engineering, Kunsan National University, Gunsan-si, Republic of Korea

ABSTRACT

This paper investigates the effects of air-void and binder content on the cracking mechanism of asphalt concrete by using induction heating. Semi-circular bending test was used to evaluate the cracking resistance of induction asphalt mixture, including fracture energy index, crack velocity, crack resistance index, and flexibility index. Compaction energy index was computed to evaluate the influence of the additive agents on the workability of asphalt mixture. Even though the healing level of asphalt mixture recovered up to 80%, cracking resistance declined greatly after one damage-healing treatment. It was observed that air void plays a major role in both healing capacity and cracking resistance, while the impact of asphalt content is milder. Furthermore, analysis results from Matlab® image processing demonstrated that the crack shape of samples was retained after induction healing, the crack area expanded approximately 18% compared to the virgin sample. The analysis also indicates that aggregate crack failure not only causes low healing level but also deteriorates cracking resistance of induction healed sample.

ARTICLE HISTORY
Received 23 March 2020
Accepted 20 September 2020

KEYWORDS
Warm mix asphalt; cracking resistance; crack propagation; healing performance; image analysis; crack detection

1. Introduction

Asphalt mixture is one of the most popular types of pavement material used worldwide (Ayar et al., 2016). This heterogeneous material includes asphalt binder, coarse, fine aggregate, filler, and additives. Nowadays, along with rapid development, the lack of material sources is an urgent problem. There are promising keys to solving this problem, such as utilising by-products as construction materials (Pham et al., 2019; Xie et al., 2013; Zeng et al., 2016), using self-healing materials (Dinh et al., 2018a), and expanding the service life (Grossegger & Garcia, 2019). Since rehabilitation consumes a high amount of fossil fuels and produces a negative impact on the environment, using self-healing asphalt mixture poses a promising solution. The investigation of the healing property of asphalt pavement has been an environmentally sustainable approach, which decreases maintenance costs and reduces greenhouse gas emissions.

Induction heating is the mainstream heating method for asphalt pavements. During the induction heating process, asphalt mixture containing conductive particles is subjected to high frequency alternating electromagnetic fields which creates an eddy current in the asphalt mixture that is electrically and magnetically susceptible (García et al., 2012). Based on Joule's law, the conductive particles in the asphalt mixture are heated by the eddy currents which then diffuse heat into the asphalt mixture, increasing the sample's temperature (Tang et al., 2016). The increase of temperature in the asphalt

CONTACT Dae-Wook Park dpark@kunsan.ac.kr

mixture is key in the healing process since bitumen is temperature-sensitive in nature. When the bitumen binder attains sufficient temperature to reduce its viscosity and fill the micro-cracks that exist within the asphalt mixture. The results of hot-mix asphalt healing by induction heating have been proved in various studies. For instance, the healing level of asphalt concrete can recover up to 85% (García et al., 2012; Hofko et al., 2015; Phan et al., 2018). This healing capacity is affected by several factors such as air void, asphalt binder type (Sun et al., 2017), heating time (García et al., 2011), and conductive particles (Phan et al., 2018). Furthermore, Dinh et al. proved that steel wool fibre (SWF) plays a specific role in the induction heating process (Dinh et al., 2018b). In addition, Norambuena-Contreras confirmed that the physical and mechanical properties of asphalt mixture containing SWF have improved. The six percent (6%), by weight of asphalt binder, is taken as an adequate dosage to archive the best healing performance and prevent clustering phenomenon (Norambuena-Contreras & Garcia, 2016).

Because of the high energy consumption and excessive greenhouse gas emission in hot-mix asphalt (HMA) production, many technologies have been developed to reduce production and construction temperature. For example, warm-mix additive significantly reduces production and construction temperature by 20–30°C. Because of the benefits of these additive agents such as binder viscosity reduction and moisture resistance improvement, they have been widely used in asphalt mixtures (Park et al., 2017). Also, Wang et al. confirmed that the viscosity of the asphalt binder strongly affected to healing performance of asphalt mastic (Wang et al., 2020). Therefore, additive agent is considered as a factor that influences asphalt healing performance. Different methods have been suggested to quantify the healing properties of asphalt. The three-point bending test is the most common method to determine the healing level because it is affordable and easily conducted in the laboratory (García et al., 2011). However, there is still inadequate research on the cracking resistance and crack propagation of healed asphalt mixture. Due to the popularity of the semi-circular bending (SCB) test, it is recommended to conduct an SCB test to resolve these issues. This test can determine (a) fracture energy necessary to cause an asphaltic mixture to crack, (b) crack velocity to evaluate a brittle or flexible mixture, (c) crack resistance index to indicate the crack behaviour of asphalt mixture, and (d) flexibility index (Kaseer et al., 2018). Finally, the formation and crack propagation have been analysed by Matlab® image processing (Hasheminejad et al., 2019).

The purpose of this research is to evaluate the impact of air-void and binder content on the cracking resistance of healed warm-mix asphalt (WMA). Two types of additive agents are utilised in the series of samples. One, warm-mix additive (D) is used to decrease mixing and compaction temperature. Two, L additive (L) is employed to increase the penetration of asphalt binder. The effect of air voids and asphalt content is also considered. Compaction energy index (CEI) is computed to evaluate the effect of the two additives on the production and construction of asphalt mixture. The SCB test assesses the healing properties of modified asphalt mixtures, then the cracking resistance of the healed sample is examined, including fracture energy (G_D), crack velocity (υ), and crack resistance index (CRI). The crack formation and crack propagation are analysed using Matlab® image processing. This research investigates and provides a better understanding the properties of healed asphalt using induction heating.

2. Materials and methods

2.1. Materials

Table 1 shows the particle size gradation of the aggregate used in making the WMA samples. The asphalt binder used in this research is PG 64-22. Steel wool fibres (SWF) were utilised as the conductive additive in the asphalt concrete mixture for induction heating (Vo et al., 2019). Also, two types of additives were considered, including warm-mix additive (D) and L additive (L). The properties of the aforementioned materials can be referred in Table 2.

Table 1. Aggregate size gradation.

Sieve size (mm)	19	12.5	9.5	4.75	2.36	0.6	0.3	0.15	0.075
Percent passing (%)	100	98	86	60	45	23	14	8	3

Table 2. Material properties.

Materials	Properties	Values	Specification
Bitumen	Density (kg/m^3)	1020	ASTM D70
	Penetration (25°C, 5 s, 0.1 mm)	70	ASTM D946
	Softening point (°C)	48	ASTM D36
Steel wool fibre	Density (kg/m^3)	7800	–
	Average length (mm)	4.25	–
	Equivalent diameter (μm)	75–130	–
	Thermal conductivity (W/m·K)	80	–
Warm mix additive (D)	Density (kg/m^3)	1000	ASTM D792
	Viscosity at 135°C (Pa-s)	0.382	ASTM D4402
	Penetration (25°C, 5 s, 0.1 mm)	75	AASHTO T 49
	Reducing temperature range(°C)	10–30	–
L additive (L)	Density (kg/m^3)	950	ASTM D792
	Viscosity at 140°C (Pa-s)	0.2 ± 0.04	ASTM D4402
	Penetration (25°C, 5 s, 0.1 mm)	73	AASHTO T 49

2.2. Sample preparation

The research flowchart is displayed in Figure 1. According to the Superpave mix design method (McGennis et al., 1995), all test specimens were prepared with three asphalt contents, varying at 0.5% from the optimum, which were 4.9%, 5.4% (optimum asphalt content – OAC), and 5.9%, by weight of the total mix. The specimens were also designed to attain three target air void values of 4%, 8%, and 12%. As for each additive, two contents of 1% and 2%, by weight of asphalt binder, were utilised. Based on previous studies, mixtures containing six percent (6%) SWF, by weight of asphalt binder, are found to accelerate the healing rate of asphalt concrete when subjected to induction heating (Dinh et al., 2018a); the same amount of SWF is used in all sample mixtures. Before mixing, aggregates and SWF are preheated in an oven for four (4) hours. Meanwhile, the binder-additive mixture is prepared for 3 h before incorporating it with the aggregates. The binder-additive mixing process includes preheating the asphalt binder for an hour. Once preheated, the additive agent is added and stirred thoroughly into the binder, then the asphalt-binder mixture is heated in the oven for two hours prior to compaction. The cylindrical samples in this study are first compacted using the Superpave Gyratory Compactor (Figure 2(a)) and have a diameter of 150 mm and a height of 160 mm, based on the semi-circular test method (AASHTO TP 124-16, 2016). Next, each compacted specimen is cut into two cylindrical slices of 50 ± 1 mm thick. Thereafter, each slice is divided into two identical 'halves' resulting in four semi-circular test specimens from each compacted cylinder. Lastly, each sample is sawed on the cut face across the midpoint of the long direction, with a notch having a depth of 15 mm and a breadth of 1.5 mm, to guide the cracking of the sample. To investigate the effect of warm mix additive (D1, D2), the mixing and compaction temperatures were reduced to 130°C and 110°C, respectively, compared to the conventional 150°C and 130°C applied with the L additive (L1, L2) and control mixtures (C0) (Panda et al., 2017). A total of 180 replicates were prepared for this study (5 additive-modified mixtures including control mix $\times$ 3 asphalt contents $\times$ 3 target air voids $\times$ 4 replicates for average).

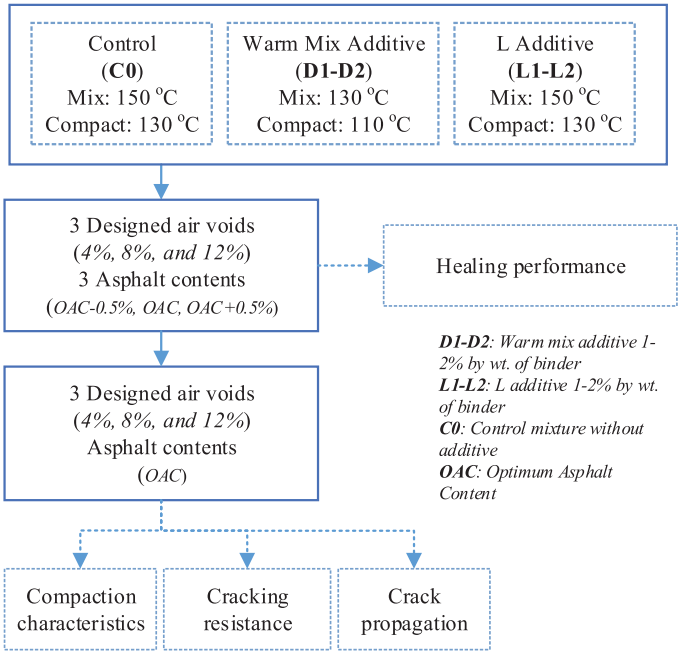

Figure 1. Research flowchart.

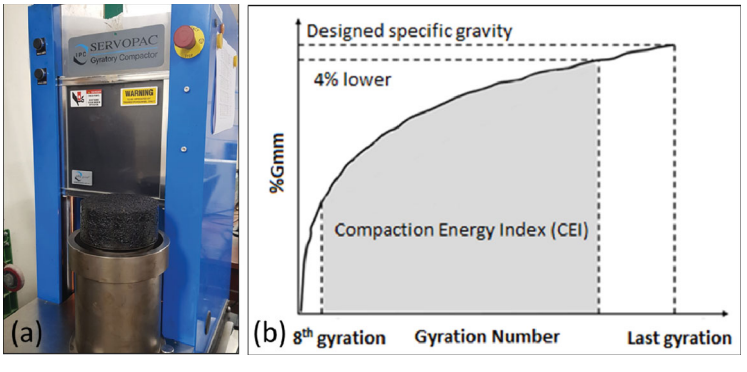

Figure 2. (a) Superpave Gyration Compactor and (b) Compaction Energy Index.

2.3. Tests and methods

2.3.1. Healing performance

After the cutting process, semi-circular samples are air-dried for 48 h to remove moisture, then conditioned in a temperature incubator at 25°C for 2 h ± 10 min before testing (AASHTO TP 124-16, 2016). The SCB test is conducted in a servo-hydraulic dynamic testing system, set to equilibrate at 25°C of chamber temperature, with a maximum load capacity of 30 kN (Figure 3(a)). Also, two LVDTs are attached to the testing jig to record the load-displacement data (Figure 3(b)). The samples are subjected to a loading rate of 50 mm/min and set to terminate when load reading drops below 0.1 kN, during which the sample has cracked. The cracked sample is then carefully removed from the jig to maintain the shape of the crack and prepare for image analysis process. After which, the cracked sample is pressed together, by hand, to bring the sample back to its original shape. The damaged samples are then let to rest for 3 h before conducting induction healing. The induction heater used in this study

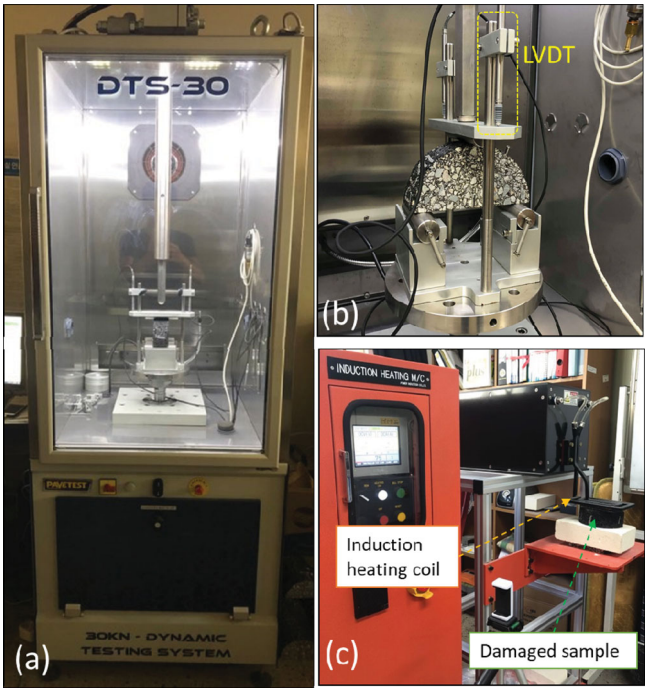

Figure 3. (a) DTS-30 machine, (b) SCB test set up, and (c) induction heating.

has a capacity of 50 kW and a maximum frequency of 35 kHz (Figure 3(c)). First, the rested damaged sample is placed under the induction heating coil and is heated until 90°C. Next, the heated or healed samples are allowed to rest for approximately 24 h to achieve ambient temperature. Then, the rested and healed samples are again conditioned in the temperature incubator for 2 h for the SCB test. This whole process equates to one damage-healing (DH) cycle.

The healing performance of the test samples was conducted until the 6th damage-healing cycle. As can be seen in Equation (1), the healing performance (H_p) of a sample is calculated by the ratio of the peak load of the healed sample at the n^{th} cycle to the peak load of the virgin sample. (Phan et al., 2018).

$$H_p = \frac{P_n}{P_0} \tag{1}$$

where P_0 is the peak load of virgin sample; P_n is peak load of healed sample at nth DH cycle

2.3.2. Compaction characteristics

The number of gyrations is recorded to calculate the compaction energy index (CEI). This test considers mixtures with three air-void content variations and optimum asphalt binder content (OAC). According to previous researches (Delgadillo & Bahia, 2008; Kim & Kang, 2018), the CEI was developed to assess compaction ability. The CEI is determined by the area under the gyration-Gmm curve, from the density at 8th gyration to 4% lower designed specific gravity in the curve (Figure 2(b)). It is found that mixtures with lower CEI values allow for easier compaction in the field. The compaction energy index can be calculated using Equation (2).

$$\mathrm{CEI} = \sum_{8}^{n_0} (n_{i+1} - n_i) \times P_i + 0.5 \times (n_{i+1} - n_i) \times (P_{i+1} - P_i) \tag{2}$$

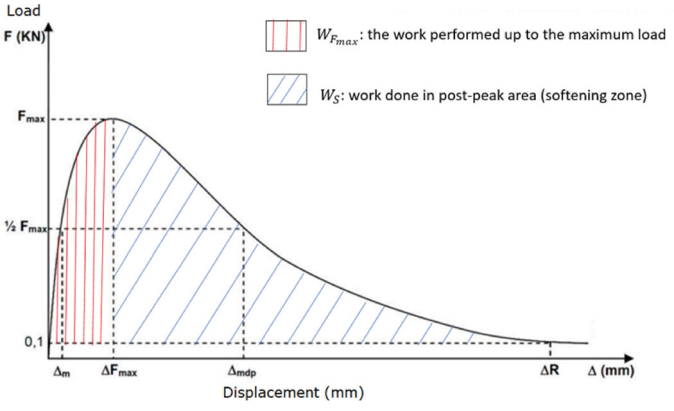

Figure 4. Load-displacement curve.

where P_i is the specific gravity corresponding to ith gyration; n_0 is the gyration at 4% lower designed specific gravity

2.3.3. Cracking resistance properties

The SCB test was also used to analyse the cracking resistance properties of modified asphalt mixtures. Figure 4 shows the load-displacement curve which can be used to compute the fracture energy (G_D), crack velocity (υ), crack resistance index (CRI), and flexibility index (FI) (Batioja-Alvarez et al., 2019). Fracture energy is one of the main cracking properties defined as the work required to initiate and propagate the crack until the sample fails. Generally, a higher G_D-value indicates better crack resistance of the asphalt mixture (AASHTO TP 124-16, 2016). Crack velocity, defined as the distance the crack travelled with respect to elapsed time, is determined by the ratio of crack length to the time elapsed. A brittle asphalt mixture presents a higher υ-value than a flexible one. Crack resistance index, taken as the total fracture energy divided by the peak load, is developed to compare two mixtures with similar G_D-values. Higher CRI magnitude indicates a better asphalt mixture in terms of resistance to cracking. Meanwhile, the flexibility index is defined as the total fracture energy divided by the slope ($|m|$) of the post-peak load at the inflection point of the load-displacement curve (Kaseer et al., 2018). The cracking properties of asphalt concrete are calculated using Equations (3) to (6), as given in Table 3. Besides, the Tukey–Kramer (T-K) statistical analysis was employed to find the difference between air voids content in terms of FI. The T-K produce is based on calculating confidence intervals for the difference between each pair of averages (μ). Each confidence interval is examined to determine if it includes zero. If the interval does not include zero, the two means are significant difference and vice versa the including zero of interval indicates the two means are not significant difference (Hess, Mason, & Gurst, 2003).

2.3.4. Crack propagation

Image analysis was used to analyse the crack propagation of virgin samples and the samples that underwent the first DH cycle. The fractured surfaces were captured using a digital camera (SONY® Cybershot DSC-HX90 V 18.1 megapixels). The camera was set on a tripod 30 cm above the target specimen. By using the MATLAB® software (Matlab R2019b, 2019), the image analysis programme was employed to detect and measure the crack area. Based on previous researches (Le et al., 2019; Otsu, 1979), the image analysis process was developed by the following steps (Figure 5):

(1) calculate the histogram of an original image
(2) find out the maximum change of pixel number and convert to grey image
(3) remove noise and detect the crack area, count total pixels of crack area
(4) convert total pixels into square millimetre

Table 3. Description of cracking properties.

Properties	Equation	Descriptions
Peak load (kN)	F_{max}	–
Displacement at peak load (mm)	ΔF_{max}	–
Fracture Energy (J/mm^2)	$G_D = \frac{W_D}{h \times l}$ (3)	$W_D = \sum_{i=1}^{n} (\Delta_{i+1} - \Delta_i) \times F_i + 0.5 \times (\Delta_{i+1} - \Delta_i) \times (F_{i+1} - F_i)$ $h = 50$(mm): the height of the specimen $l = 60$ (mm): the original ligament length of the specimen
Crack velocity (mm/s)	$\upsilon = \frac{\Delta l}{\Delta t}$ (4)	Δl(mm): the length of the crack Δt(s): the time elapsed
Crack resistance index(J/kNmm^2)	$CRI = \frac{G_D}{\lvert F_{max} \rvert}$ (5)	G_D (J/mm^2): fracture energy F_{max}(kN): peak load
Flexibility index	$FI = \frac{G_D}{\lvert m \rvert} \times 0.01$ (6)	G_D (J/mm^2): fracture energy $\lvert m \rvert$: slope at the inflection point of post-peak load versus displacement curve

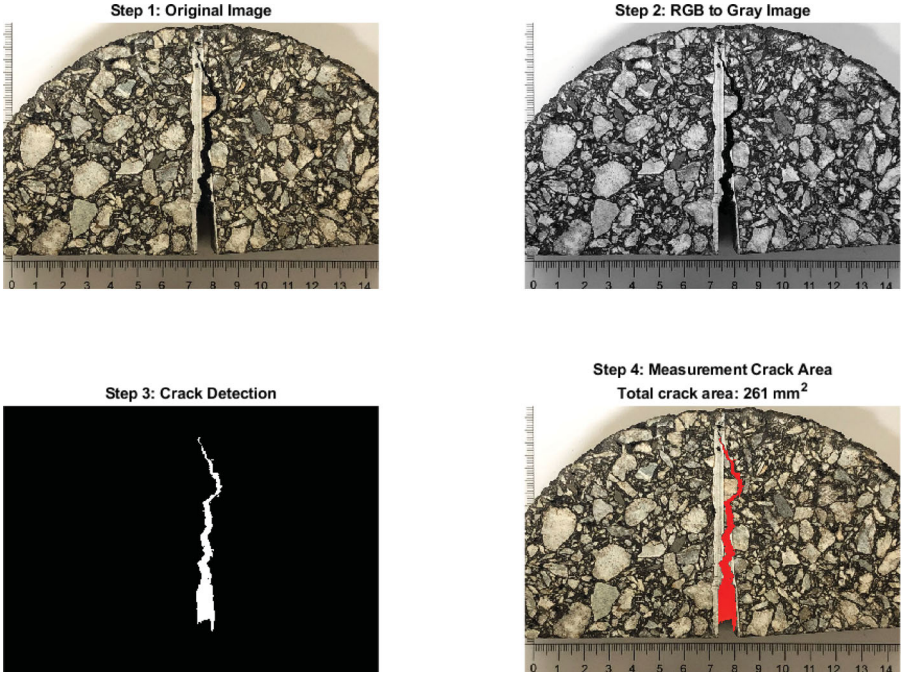

Figure 5. Image analysis process.

3. Results and discussion

3.1. Healing performance

Figure 6 illustrates the healing level of asphalt mixtures. For each mixture, the bar graph shows healing performance at the 1st, 3rd, and 6th DH cycles. Overall, the healing level gradually decreases with an increase in DH cycle and eventually declines by 30% compared to the first cycle when it reaches the sixth cycle. This may be due to the effect of the repeated damage-healing cycles that resulted in the aging of the binder, leading to the deteriorating adhesion between the binder and aggregate (Dinh et al., 2018b; Phan et al., 2018). Moreover, air void content strongly affected the healing level results (Salih et al., 2018). The four percent (4%) AV mixture displayed the highest healing level among three designed air voids. For every 4% additional air void on the asphalt mixture, the healing results are

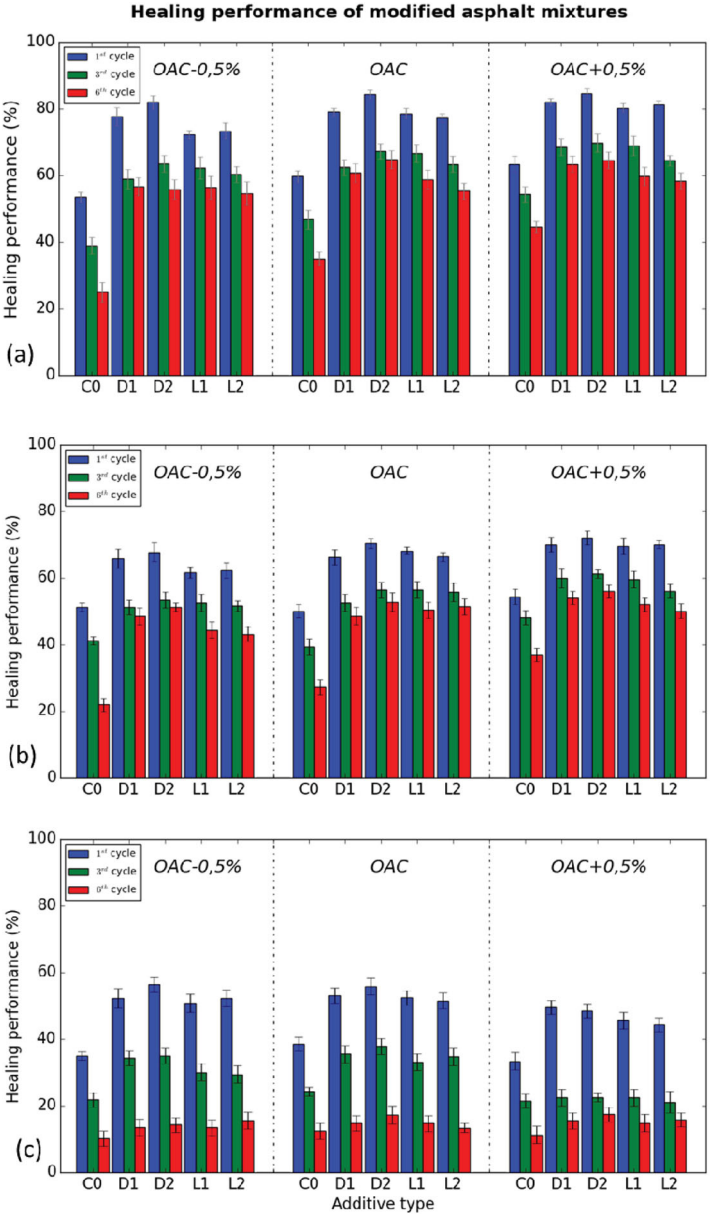

Figure 6. Healing performance of asphalt mixtures with (a) 4% air voids, (b) 8% air voids, and (c) 12% air voids.

reduced approximately by ten percent (10%). This is due to the discontinuities in the asphalt structure which hinders heat transfer in the samples with bigger air void contents (Li et al., 2019).

As for the effect of asphalt content, the test results indicated that its effect is negligible. There were three asphalt binder dosages developed to evaluate the effect of asphalt content on healing performance and the outcomes showed that there was not much difference among the three asphalt contents. Increasing the binder by a margin of 0.5% helps improve healing results only by approximately three percent (3%).

Among five differential mixtures, samples with warm-mix additive (D) showed the best healing level in either air voids or asphalt content. In the first DH cycle, the healing levels of D-samples reached

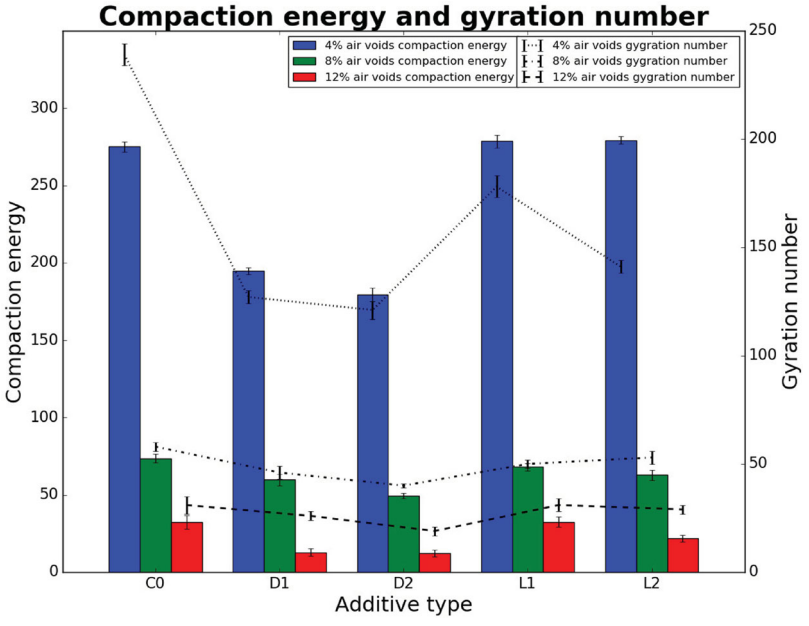

Figure 7. Compaction energy and gyration number of modified mixtures with optimum asphalt content.

higher than 80% and reduced to 65% and 60% after the third and sixth cycles, respectively. On the other hand, the mixtures with L additive presented a 5% lower healing result than the warm mix additive. Compared to other contents, two percent (2%) additive content helped the asphalt mixtures gain a higher healing level. The beneficial effect of warm-mix additive (D) to the healing level can be explained by its primary purpose: reduction of mixing and compaction temperatures by 20°C. Because of this, the samples with 2% of D additive (D2) yielded better healing performance since the binder is more susceptible to lower temperatures. This caused the bitumen to increase its penetration and helped it to flow easily and fill cracks upon reaching 90°C of maximum induction heating. The higher penetration helps bitumen to easily flow and fill the cracks (Lee et al., 2019), healing the asphalt by recovering the lost bond between aggregate and binder. As a result, the D additive has more effect on the healing performance of asphalt mixture than the L additive, and all samples with additives out-performed the control samples.

3.2. Compaction characteristics

Figure 7 presents the compaction energy and gyration number of modified asphalt mixtures. Expectedly, the lower air void design mixtures required a higher number of gyrations to achieve the desired air void. The D1 mixtures with 4% air void required 127 gyrations compared to that of the 8% and 12% air void mixtures, which needed 46 and 26 gyrations, respectively. Related studies have noted that warm mix additive reduces the strong adhesion between aggregates during the compaction process because it acts as a lubricant (Pereira et al., 2018). Consequently, the mixtures containing warm mix additive reduced CEI even though mix and compact temperature were already reduced at 130°C and 110°C, respectively. Also, it can be observed that the CEI declined three times with each 4% increase in air void.

On the other hand, the L additive slightly improved the penetration of bitumen with 73 (mm/10 s) compared to 70 (mm/10 s) of the original binder. This slight difference causes insignificant change in CEI values between the L mixtures and control mixtures. It was observed that mixtures with a higher

Table 4. Cracking properties of virgin samples.

	Mixture	F_{max} (kN)	ΔF_{max} (mm)	υ (mm/s)	G_D (J/mm^2)	CRI (J/kNmm^2)	FI
4% AV	C0	3.02	1.13	5.87	1915.25	634.19	5.53
	D1	3.63	1.31	5.13	2248.60	619.45	4.91
	D2	3.35	1.29	5.73	2431.76	725.90	4.80
	L1	3.26	1.08	5.35	1975.07	605.85	5.12
	L2	3.39	1.17	5.93	2080.17	613.62	4.72
8% AV	C0	3.06	1.04	6.76	1555.57	508.36	8.92
	D1	3.11	1.01	6.35	1915.08	615.78	8.06
	D2	3.02	1.13	6.48	2148.30	711.36	8.09
	L1	2.92	1.63	6.47	1915.10	655.86	8.22
	L2	3.03	1.49	6.41	2028.38	669.43	7.96
12% AV	C0	2.45	1.26	7.22	1250.06	510.23	12.80
	D1	2.78	1.39	7.69	1369.93	492.78	10.69
	D2	2.61	1.45	7.15	1510.58	578.77	11.42
	L1	2.42	1.43	7.86	1231.53	508.90	11.32
	L2	2.40	1.64	7.10	1367.69	569.87	10.61

additive content would obtain lower CEI values. The higher additive content helps sufficient workability of asphalt mixture during the compaction process (Yu et al., 2018). For both additive types, the CEI of mixtures with two percent additives (D2, L2) were around 7% lower than that of one percent (D1, L1).

3.3. Cracking resistance properties

Since the varying binder content of 0.5% showed slight improvements in healing, Table 4 and Table 6 only present the cracking properties of asphalt mixture with optimum asphalt content. Noticeably, the asphalt mixtures with lower air void gained higher peak loads. The peak load of 4% air void mixtures ranged from 3.3 to 3.6 kN, whereas the 8% and 12% air void mix attained 2.8 to 3.1 kN and 2.4 to 2.8 kN, respectively. Inversely, the fracture energy decreased with an increase in air void content. The 4% AV mixtures presented the best crack resistance, with G_D values ranging from 1915 to 2431 J/mm^2. Among the five additive mixture variations, the highest G_D was recorded from the virgin D2 mixture. Additionally, containing two percent of warm mix additive helped enhance fracture energy by 456 J/mm^2 compared to the control mixture. Moreover, the L additive mixtures had a slight improvement in their cracking properties: a 12% increase in peak load and 5% in fracture energy. As for the crack velocity, the results showed similar behaviour to previous studies where the υ –value is increased with increasing air void content (Tarefder et al., 2009). The control mixture presented the highest crack velocity which indicated a greater crack susceptibility compared to mixtures with additive. Also, the higher crack resistance index (CRI) would indicate a better asphalt mixture in terms of resistance to cracking (flexible mixture). The D2 mixture archived the highest CRI, which was 725.90, compared to 634.19 of the control mixtures. Moreover, mixtures with higher air void contents presented a greater flexibility indices (FI). This phenomenon can be explained by previous observations where the increase in air voids leads to a decrease in the post-peak slope ($|m|$), resulting in higher FI (Kaseer et al., 2018). Although, at the same air void content, mixtures containing D additive has a slightly improved FI compared to L additive mixtures. The statistical results from the Tukey–Kramer method show that there was a significant difference among the three air void contents in terms of flexibility index (Table 5). In order words, the flexibility index is dependent on the air void content of the sample.

Table 6 shows the cracking properties of the samples after one healing cycle. Generally, the cracking resistance of damaged-healed samples is decreased by approximately 50% compared to virgin samples. The 4% AV mixtures gained higher CRI values than the 8% and 12% AV mixtures. The sharp decline in fracture energy indicates a weak crack resistance of the healed mixture although, its healing

Table 5. Flexibility Index multiple comparisons by T-K procedure (studentized $q = 0.05$).

	T-K interval		
Comparisons	Lower value	Higher value	Conclusions
4% AV to 8% AV	−4.304	−1.766	Significantly different
4% AV to 12% AV	−7.421	−4.883	Significantly different
8% AV to 12% AV	−4.386	−1.848	Significantly different

Table 6. Cracking properties of healed samples after one healing cycle.

	Mixture	F_{max} (kN)	ΔF_{max} (mm)	υ (mm/s)	G_D (J/mm^2)	CRI (J/kNmm^2)	FI
4% AV	C0	2.49	0.52	8.37	659.63	264.91	2.21
	D1	2.63	0.68	7.23	821.60	312.40	2.19
	D2	2.55	0.54	7.18	687.02	269.42	3.28
	L1	2.48	0.53	7.12	796.80	321.29	3.01
	L2	2.41	0.66	7.82	804.58	333.85	2.97
8% AV	C0	0.85	0.43	11.65	201.08	236.56	4.92
	D1	1.81	0.40	10.27	228.05	125.99	5.26
	D2	1.87	0.37	10.18	356.84	190.82	6.09
	L1	1.66	0.33	10.67	190.14	114.54	5.22
	L2	1.31	0.31	10.32	143.79	109.76	6.96
12% AV	C0	0.88	0.49	14.02	364.14	413.80	7.22
	D1	1.16	0.47	13.14	463.51	399.58	6.76
	D2	0.89	0.50	12.98	365.87	411.09	7.56
	L1	1.29	0.52	13.03	499.52	387.22	8.87
	L2	0.33	0.42	13.28	195.86	593.52	7.99

level reached 80%. This phenomenon may be explained by the presence of air cells in the crack line of the sample that was caused by inadequate healing of the asphalt mastic. These air cells play a role as 'pre-cracks' or discontinuities in the asphalt mixture, which are quickly extended when the load is applied. The crack velocity reinforces this hypothesis. The crack velocity of the healed samples was twice as high than that of the virgin samples. Consequently, the CRI and FI also declined after the first damage-healing (DH) cycle.

3.4. Crack propagation

Figure 8 presents the crack areas of the asphalt mixtures at 0 and the 1st DH cycle. It can be observed that the crack area increases with an increase in DH cycle. For example, the control (C0) mixture with 4% AV attained 323 mm^2 areas at 0 cycles which increased to 352 mm^2 after one DH cycle. The samples with higher air void content resulted with larger crack areas because of the lack of connection between mixture particles. As mentioned in Section 3.3, the presence of these air voids causes the particle discontinuity which deteriorates the cracking resistance of asphalt mixture. Among the five mixtures, the D2 sample gained the lowest crack areas of 247, 278, and 305 mm^2 at 4%, 8%, and 12% of air void, respectively.

As can be observed in Figure 9, the crack shape of the samples were retained, but the crack area expanded up to 18% after one DH treatment. This phenomenon can be confirmed by the fact that a crack-healed asphalt sample is weaker than its original asphalt base (Wang et al., 2013). This can also be confirmed by the deteriorating cracking properties of the samples after the succeeding DH cycles. Figure 10 illustrates two common crack failures that occur in asphalt concrete: aggregate crack and base asphalt crack. In this research, most of the aggregate crack failures were recorded in the lower air void mixtures. An aggregate crack failure would sharply deteriorate the cracking properties and the healing level of asphalt mixture. Table 7 presents the decline of cracking properties of the asphalt mixture after the 1st DH cycle, comparing the effects of aggregate crack and base asphalt crack failure. The fracture energy was approximately four times lower with aggregate crack failure, while the velocity

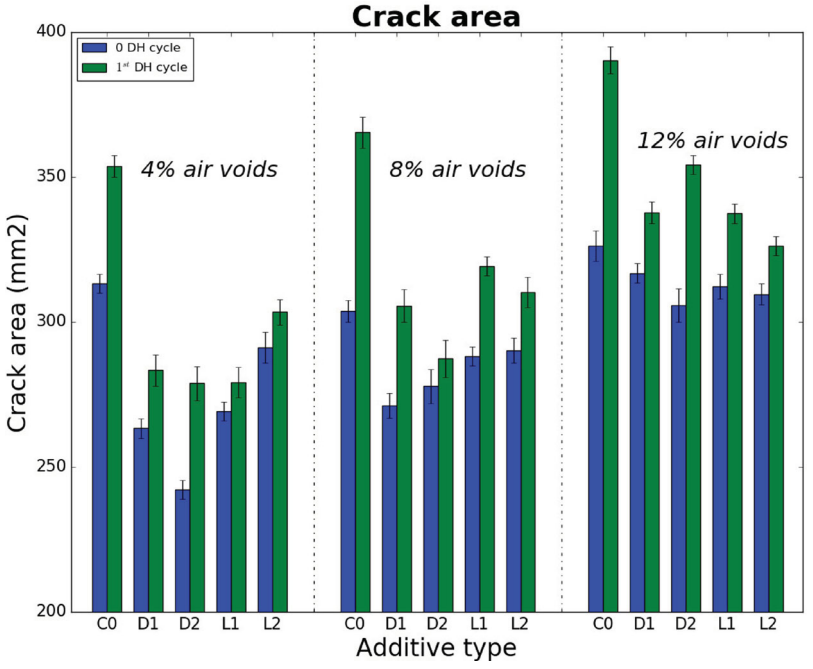

Figure 8. Crack area of asphalt mixtures at 0 at 1st DH cycle.

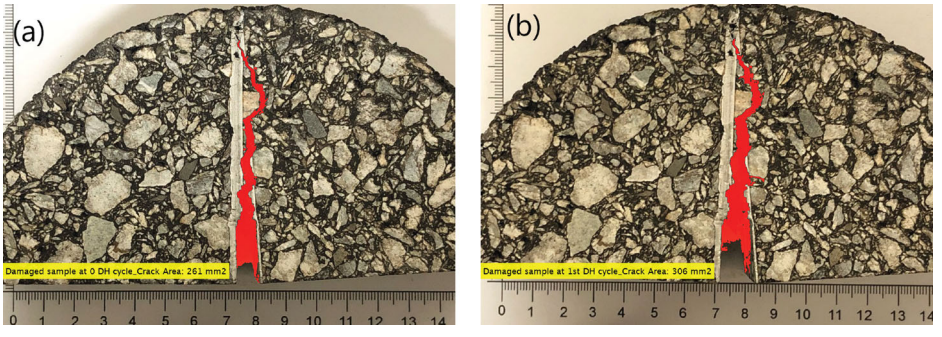

Figure 9. Crack expansion of (a) virgin sample and (b) healed sample.

Table 7. Deterioration of cracking properties based on crack failure of asphalt mixture.

Crack failure	F_{max} (kN)	ΔF_{max} (mm)	ΔR (mm)	υ (mm/s)	G_D (J/mm^2)	CRI (J/kNmm^2)
Aggregate crack	0.55	0.23	1.26	11.18	115.02	209.09
Base asphalt crack	2.55	0.54	2.00	7.18	687.02	269.42

crack nearly doubled compared to the base asphalt crack sample. This can be concluded that asphalt mixtures having aggregate crack failure could not be recovered by induction heating. Figure 11 shows the crack shape of two types of air void. With a 15 mm notch, the 4% air void mixture exhibited a straight-line crack, while the 12% air void sample attained a curve crack. This was expected to happen since several weak spots in the asphalt mixture redirect the propagation of cracks (Zeng et al., 2016).

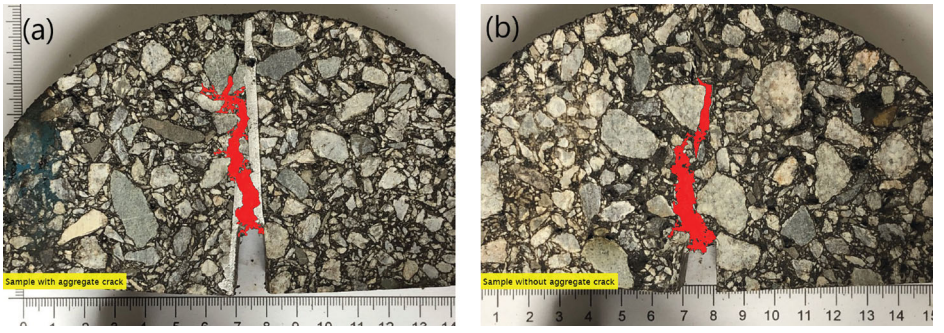

Figure 10. Asphalt mixture (a) with aggregate crack failure and (b) without aggregate crack failure.

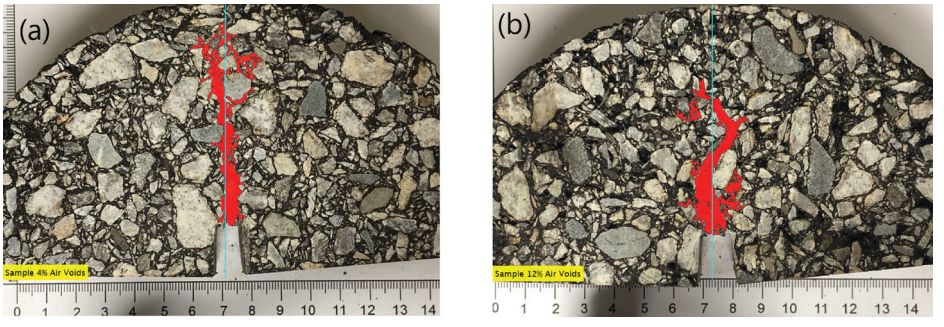

Figure 11. The crack shape of (a) 4% air voids sample and (b) 12% air voids sample.

4. Conclusions

In this research, the cracking resistance of healed warm mix asphalt based on air-void, and binder contents was investigated. The SCB test was employed to conduct a series of tests on sample replicates. The cracking resistance properties before and after induction healing were analysed as well. By using Matlab® image analysis, the crack propagation of the asphalt mixtures was investigated. Conclusions drawn from the study are summarised below:

- For every 4% increase in the air void, the healing level approximately decreases by 10%, whereas the impact of asphalt content is milder. Increasing the binder content by a margin of 0.5% helps improve healing results slightly by approximately 3%.
- Even though the healing level can be recovered up to 80%, the cracking resistance property of the asphalt mixture strongly declines after one damage-healing (DH) cycle.
- The results from Tukey–Kramer show that AV content plays a major role in the cracking resistance of asphalt mixture. The higher AV content leads to a greater flexibility index (FI).
- The crack shape of healed samples is retained after succeeding damage-healing (DH) cycles; meanwhile, the crack area expanded to approximately 18%. This phenomenon indicates that the crack healed is weaker than the original base asphalt.
- Aggregate crack failure in asphalt mixture not only causes a decrease in the healing level, but also sharply deteriorates the cracking properties of the asphalt mixture.
- The crack shape of high air void content (12%) is curved compared to the straight cracks in the 4% air void mixture, due to the local weakness of the asphalt mixture.

Disclosure statement

No potential conflict of interest was reported by the author(s).

Funding

This research was supported by Basic Science Research Program through the National Research Foundation of Korea funded by the Ministry of Education of the Republic of Korea (No. NRF-2017R1D1A1B03032594).

ORCID

Tam Minh Phan http://orcid.org/0000-0001-8696-9207

References

AASHTO TP 124-16. (2016). Provisional standard method of test for determining the fracture potential of asphalt mixtures using semicircular bend geometry (SCH) at intermediate temperature.

Ayar, P., Moreno-Navarro, F., & Rubio-Gámez, M. C. (2016). The healing capability of asphalt pavements: A state of the art review. *Journal of Cleaner Production*, *113*, 28–40. https://doi.org/10.1016/j.jclepro.2015.12.034

Batioja-Alvarez, D., Lee, J., & Haddock, J. E. (2019). Understanding the Illinois flexibility index test (I-FIT) using Indiana asphalt mixtures. *Transportation Research Record: Journal of the Transportation Research Board*, *2673*(6), 337–346. https://doi.org/10.1177/0361198119841282

Delgadillo, R., & Bahia, H. U. (2008). Effects of temperature and pressure on hot mixed asphalt compaction: Field and laboratory study. *Journal of Materials in Civil Engineering*, *20*(6), 440–448. https://doi.org/10.1061/(ASCE)0899-1561(2008)20:6(440)

Dinh, B. H., Park, D.-W., & Le, T. H. M. (2018a). Effect of rejuvenators on the crack healing performance of recycled asphalt pavement by induction heating. *Construction and Building Materials*, *164*(6), 246–254. https://doi.org/10.1016/j.conbuildmat.2017.12.193

Dinh, B. H., Park, D.-W., & Phan, T. M. (2018b). Healing performance of granite and steel slag asphalt mixtures modified with steel wool fibers. *KSCE Journal of Civil Engineering*, *22*(6), https://doi.org/10.1007/s12205-018-1660-8

García, Á, Schlangen, E., van de Ven, M., & Liu, Q. (2012). A simple model to define induction heating in asphalt mastic. *Construction and Building Materials*, *31*, 38–46. https://doi.org/10.1016/j.conbuildmat.2011.12.046

García, Á, Schlangen, E., van de Ven, M., & van Vliet, D. (2011). Induction heating of mastic containing conductive fibers and fillers. *Materials and Structures*, *44*(2), 499–508. https://doi.org/10.1617/s11527-010-9644-2

Grossegger, D., & Garcia, A. (2019). The effect of water and pressure on the self-healing of macro cracks in asphalt mortar beams. *Construction and Building Materials*, *229*. Article 116941. https://doi.org/10.1016/j.conbuildmat.2019.116941

Hasheminejad, N., Vuye, C., Margaritis, A., Ribbens, B., Jacobs, G., Blom, J., Van den bergh, W., Dirckx, J., & Vanlanduit, S. (2019). Investigation of crack propagation and healing of asphalt concrete using digital image correlation. *Applied Sciences*, *9*(12), 2459. https://doi.org/10.3390/app9122459

Hess, J. L., Mason, R. L., & Gurst, R. F. (2003). *Statistical design and analysis of experiments: With applications to engineering and science* (2nd ed.).

Hofko, B., Handle, F., Eberhardsteiner, L., Hospodka, M., Blab, R., Füssl, J., & Grothe, H. (2015). Alternative approach toward the aging of asphalt binder. *Transportation Research Record: Journal of the Transportation Research Board*, *2505*(1), 24–31. https://doi.org/10.3141/2505-04

Kaseer, F., Yin, F., Arámbula-Mercado, E., Epps Martin, A., Daniel, J. S., & Salari, S. (2018). Development of an index to evaluate the cracking potential of asphalt mixtures using the semi-circular bending test. *Construction and Building Materials*, *167*, 286–298. https://doi.org/10.1016/j.conbuildmat.2018.02.014

Kim, K., & Kang, M. (2018). Linking the effect of aggregate interaction to the compaction theory for asphalt mixtures using image processing. *Applied Sciences*, *8*(11), https://doi.org/10.3390/app8112045

Le, T. H. M., Park, D.-W., Park, J.-Y., Phan, T. M., & Liu, Q. (2019). Evaluation of the effect of fly ash and slag on the properties of cement asphalt mortar. *Advances in Materials Science and Engineering*, *2019*, https://doi.org/10.1155/2019/1829328

Lee, S.-H., Tam, A. B., Kim, J., & Park, D.-W. (2019). Evaluation of rejuvenators based on the healing and mechanistic performance of recycled asphalt mixture. *Construction and Building Materials*, *220*, 628–636. https://doi.org/10.1016/j.conbuildmat.2019.05.150

Li, H., Yu, J., Wu, S., Liu, Q., Li, B., Li, Y., & Wu, Y. (2019). Study on the gradient heating and healing behaviors of asphalt concrete induced by induction heating. *Construction and Building Materials*, *208*, 638–645. https://doi.org/10.1016/j.conbuildmat.2019.03.052

Matlab R2019b (MATLAB R2019b). (2019). https://www.mathworks.com/

McGennis, R. B., Anderson, R. M., Kennedy, T. W., & Solaimanian, M. (1995, February). *Background of superpave asphalt mixture design and analysis*. FHWA-SA-95-003, 160.

Norambuena-Contreras, J., & Garcia, A. (2016). Self-healing of asphalt mixture by microwave and induction heating. *Materials & Design*, *106*, 404–414. https://doi.org/10.1016/j.matdes.2016.05.095

Otsu, N. (1979). A threshold selection method from gray-level histograms. *IEEE Transactions on Systems, Man, and Cybernetics*, *9*(1), 62–66. https://doi.org/10.1109/TSMC.1979.4310076

Panda, M., Padhi, M. M., & Giri, J. P. (2017). Use of emulsion for warm mix asphalt. *International Journal of Transportation Science and Technology*, *6*(1), 78–85. https://doi.org/10.1016/j.ijtst.2017.04.001

Park, D.-W., Seo, W.-J., Kim, J., & Vo, H. V. (2017). Evaluation of moisture susceptibility of asphalt mixture using liquid anti-stripping agents. *Construction and Building Materials*, *144*, 399–405. https://doi.org/10.1016/j.conbuildmat.2017.03.214

Pereira, R., Almeida-Costa, A., Duarte, C., & Benta, A. (2018). Warm mix asphalt: Chemical additives' effects on bitumen properties and limestone aggregates mixture compactibility. *International Journal of Pavement Research and Technology*, *11*(3), 285–299. https://doi.org/10.1016/j.ijprt.2017.10.005

Pham, V. A. K., Nguyen, K. T., Le, A. T., Han, W. S., Lee, G., & Lee, K. (2019). Assessment of performance of fiber reinforced geopolymer composites by experiment and simulation analysis. *Applied Sciences*, *9*(16), https://doi.org/10.3390/app9163424

Phan, T. M., Park, D.-W., & Le, T. H. M. (2018). Crack healing performance of hot mix asphalt containing steel slag by microwaves heating. *Construction and Building Materials*, *180*, 503–511. https://doi.org/10.1016/j.conbuildmat.2018.05.278

Salih, S., Gómez-Meijide, B., Aboufoul, M., & Garcia, A. (2018). Effect of porosity on infrared healing of fatigue damage in asphalt. *Construction and Building Materials*, *167*, 716–725. https://doi.org/10.1016/j.conbuildmat.2018.02.065

Sun, D., Yu, F., Li, L., Lin, T., & Zhu, X. Y. (2017). Effect of chemical composition and structure of asphalt binders on self-healing. *Construction and Building Materials*, *133*, 495–501. https://doi.org/10.1016/j.conbuildmat.2016.12.082

Tang, J., Liu, Q., Wu, S., Ye, Q., Sun, Y., & Schlangen, E. (2016). Investigation of the optimal self-healing temperatures and healing time of asphalt binders. *Construction and Building Materials*, *113*, 1029–1033. https://doi.org/10.1016/j.conbuildmat.2016.03.145

Tarefder, R. A., Kias, E. M., & Ng, T. (2009). Factors affecting cracking of notched asphalt concrete. *International Journal of Pavement Research and Technology*, *2*(4), 137–147. https://doi.org/10.6135/ijprt.org.tw/2009.2(4).137

Vo, H. V., Park, D.-W., Seo, J.-W., & Le, T. H. M. (2019). Effects of asphalt types and aging on healing performance of asphalt mixtures using induction heating method. *Journal of Traffic and Transportation Engineering (English Edition)*, https://doi.org/10.1016/J.JTTE.2018.10.009

Wang, R., Qi, Z., Li, R., & Yue, J. (2020). Investigation of the effect of aging on the thermodynamic parameters and the intrinsic healing capability of graphene oxide modified asphalt binders. *Construction and Building Materials*, *230*. Article 116984. https://doi.org/10.1016/j.conbuildmat.2019.116984

Wang, H., Zhang, C., Yang, L., & You, Z. (2013). Study on the rubber-modified asphalt mixtures' cracking propagation using the extended finite element method. *Construction and Building Materials*, *47*, 223–230. https://doi.org/10.1016/j.conbuildmat.2013.05.035

Xie, Z., Fan, W., Wang, L., & Shen, J. (2013). The effectiviness of warm mix asphalt (WMA) additives affected by the type of aggregate and binder. *International Journal of Pavement Research and Technology*, *6*, 554–561. https://doi.org/10.6135/ijprt.org.tw/2013.6(5).554

Yu, H., Leng, Z., Dong, Z., Tan, Z., Guo, F., & Yan, J. (2018). Workability and mechanical property characterization of asphalt rubber mixtures modified with various warm mix asphalt additives. *Construction and Building Materials*, *175*, 392–401. https://doi.org/10.1016/j.conbuildmat.2018.04.218

Zeng, G., Yang, X., Chen, L., & Bai, F. (2016). Damage evolution and crack propagation in semicircular bending asphalt mixture specimens. *Acta Mechanica Solida Sinica*, *29*(6), 596–609. https://doi.org/10.1016/S0894-9166(16)30330-5